



Pergamon

Available online at www.sciencedirect.comwww.actamat-journals.com

Acta Materialia XX (2003) XXX–XXX

Computer simulation of spinodal decomposition in constrained films

D.J. Seol^{a,b,*}, S.Y. Hu^b, Y.L. Li^b, J. Shen^c, K.H. Oh^a, L.Q. Chen^b^a School of Materials Science and Engineering and Research Institute of Advanced Materials, Seoul National University, San 56-1, Shinrim-dong, Gwanak-gu, Seoul 151-742, South Korea^b Department of Materials Science and Engineering, The Pennsylvania State University, University Park, PA 16802, USA^c Department of Mathematics, Purdue University, West Lafayette, IN 47907, USA

Received 7 February 2003; received in revised form 30 June 2003; accepted 2 July 2003

Abstract

The morphological evolution during spinodal decomposition of a binary alloy thin film elastically constrained by a substrate is studied. Elastic solutions, derived for elastically anisotropic thin films subject to the mixed stress-free and constraint boundary conditions, are employed in a three-dimensional phase-field model. The Cahn–Hilliard diffusion equation for a thin film boundary condition is solved using a semi-implicit Fourier-spectral method. The effect of composition, coherency strain, film thickness and substrate constraint on the microstructure evolution was studied. Numerical simulations show that in the absence of coherency strain and substrate constraint, the morphology of decomposed phases depends on the film thickness and the composition. For a certain range of compositions, phase separation with coherency strain in an elastically anisotropic film shows the behavior of surface-directed spinodal decomposition driven by the elastic energy effect. Similar to bulk systems, the negative elastic anisotropy in the cubic alloy results in the alignment of phases along $\langle 1\ 0\ 0 \rangle$ elastically soft directions.

© 2003 Acta Materialia Inc. Published by Elsevier Ltd. All rights reserved.

Keywords: Spinodal decomposition; Thin film; Strain energy; Anisotropy; Phase-field model

1. Introduction

Spinodal decomposition takes place through spontaneous amplification of compositional fluctuations when a quenched homogeneous phase annealed within a miscibility gap becomes unstable with respect to phase separation into two phases

with different compositions. Since new phases form by a continuous process, interfaces between the two phases remain coherent during phase separation [1]. Formation of coherent microstructures generates elastic strain energy whose magnitude depends on the degree of lattice mismatch, the elastic properties of each phase, and the spatial distributions of coherent domains [2]. Since Cahn first introduced the elastic energy contribution to spinodal decomposition [3], there have been many studies on the thermodynamics of coherent systems [2,4–22]. There have been a number of theoretical

* Corresponding author. Tel.: +1-814-865-0389; fax: +1-814-865-2917.

E-mail address: sxd42@psu.edu (D.J. Seol).

studies on the spinodal phase separation in confined geometries such as thin films or plates [23–25]. It was shown that the growth of A-rich and B-rich domains and their morphology in a confined binary system is distinctly modified compared to those in the bulk [26]. Most of the existing studies are, however, on confined fluid systems or in solid thin films in which the elastic energy is ignored. In this work, we consider a thin solid film constrained by a much thicker substrate. The average lattice mismatch and/or the difference in thermal expansion coefficients between the film and the substrate causes strain energy in addition to the coherency strain energy due to compositional inhomogeneity in the film. A uniform substrate constraint from the average lattice mismatch may change the equilibrium volume fractions of decomposed phases. A periodic substrate constraint from highly ordered arrays of misfit dislocations in the substrate may control the wavelength of spinodal decomposition in a thin film [27]. A patterned substrate can significantly affect spinodally decomposed two-phase microstructures and may provide monolayers of periodic nanostructures from an initially homogeneous alloy [28]. As the film thickness increases, dislocations form at the film/substrate interface to reduce the strain energy. The local stress field near interfacial dislocations may affect the decomposition kinetics, hence the morphology [29]. If the film thickness is comparable to the substrate thickness so that the substrate is compliant to the stressed thin film, the substrate affects the stress state in the film through both the average misfit strain and the bending stiffness of the layered system [30].

The presence of the surface and interface breaks translational and rotational symmetry. As a result, a given component may prefer to occupy the surface or interface sites to produce low surface/interface energy, resulting in the so-called surface-directed spinodal decomposition [31]. In this mechanism, an enriched surface layer of the preferred component is followed by an adjacent depletion layer, and the spinodal wave will grow with a dominant wave vector directed normal to the surface. Several recent simulations have reported both the development of alternating layers of the phases lying parallel to the surface as well

as the formation of rows of particles parallel to the surface, taking into account the dependence of the surface energy on composition [32–34]. Temperature history of the system, for example, cooling from the outside surface, may also cause the surface-directed spinodal decomposition [35]. We will show that the coherency strain energy in a thin film can cause the spinodal decomposition of surface-directed characteristics.

Phase separation in a thin solid film should consider both the effect of the strain energy due to compositional self-strain and substrate constraint, and the effect of the surface/interface energy. In this paper, we extend the phase-field approach using the Cahn–Hilliard-type diffusion equation to describe a three-dimensional morphological evolution during a spinodal decomposition and coarsening in a thin film attached to a substrate at constant temperature. The phase-field approach provides a convenient basis for the numerical solution of complicated pattern evolution of transforming phases. There is no a priori assumption for the evolution. In our model, the film is assumed to be a binary (AB) alloy with two equilibrium phases. We assume the diffusion only occurs in the film, the substrate is sufficiently thick compared to the film thickness, and the interface is coherent. Elastic solutions are derived for the elastically anisotropic thin films subject to the mixed stress-free and constraint boundary conditions. These thin film boundary conditions have been successfully applied to the phase-field simulation of the formation of martensitic domains [36–38]. Elastic solutions from thin film boundary conditions are employed in a three-dimensional phase-field model. We study the dependence of morphological evolution on the coherency strain, elastic anisotropy, thin film thickness and the composition. The surface and interface contributions to the total free energy are not included, which would modify the thermodynamics near the surface [26] and appear as part of the boundary conditions at the surface and interface. The effect of surface and interface contributions will be studied in the sequels to this paper. We also would like to point out another important assumption that the surface and interface are essentially flat only allowing elastic displacements. This assumption prevents the

morphological changes due to the surface energy driven evolution near the surface region, e.g. the formation of triple junctions between the surfaces of α and β phases and the α/β interphase boundary with the junction angles determined by the surface and interphase boundary energies. Therefore, it is important to stress that the relaxation of this assumption may significantly change the morphologies predicted in this work and will be studied in our future work. On the other hand, this assumption allows us to isolate the effect of the stress-free surface and constrained interface on the morphological development without the complexity of surface-energy driven morphological changes. Finally, the film is assumed to be elastically homogeneous and has the same elastic modulus as the substrate. As a result, the effect of the substrate constraint on the film morphology is significant only near the surface where the stress is zero and near the interface where it is constrained by the substrate. Due to this homogeneous modulus approximation, the substrate constraint has no effect on the two-phase morphology inside the film just like in a three-dimensional bulk system the applied stress or strain has no effect on the morphology if the modulus is homogeneous.

2. Phase-field model

2.1. Kinetic evolution equation

To describe the temporal evolution of a composition field, we employ the Cahn–Hilliard diffusion equation,

$$\frac{\partial X}{\partial t} = \nabla \cdot \left[M \nabla \left(\frac{\delta F}{\delta X} \right) \right] \quad (1)$$

where X is the composition of species 2 (mole or atom fraction), F is the total free energy of a system. If we assume that the atomic mobilities of species 1 and 2 are equal, the mobility, M , is given by [39]

$$M = \frac{DX(1-X)}{k_B T} \quad (2)$$

where D is the diffusion coefficient, k_B is the

Boltzmann constant and T is the temperature. The mobility is further simplified by assuming that the factor $X(1-X)$ is a constant given by $X_0(1-X_0)$ where X_0 is the overall composition.

Because the total free energy in Eq. (1) includes the bulk chemical free energy, interfacial energy and elastic energy, we have

$$\frac{\partial X}{\partial t} = \nabla \cdot \left[\frac{DX_0(1-X_0)}{k_B T} \nabla \left(\frac{df(X)}{dx} - \alpha \nabla^2 X + \mu_{el} \right) \right] \quad (3)$$

where f is the bulk chemical free energy density, α is the gradient energy coefficient which is related to the interfacial energy, and μ_{el} is the elastic potential which is the derivative of the elastic energy with respect to the composition.

Using reduced variables we have the dimensionless form of the kinetic equation:

$$\frac{\partial X(\bar{r}^*, t^*)}{\partial t^*} = (\nabla^*)^2 \left(\frac{df^*(X)}{dX} - \alpha^* (\nabla^*)^2 X + \mu_{el}^* \right) \quad (4)$$

where $r^* = r/l_0$, $t^* = DtX_0(1-X_0)/l_0^2$, $\nabla^* = l_0^2 \nabla$, $f^* = f/(k_B T)$, $\alpha^* = \alpha/(k_B T l_0^2)$ and $\mu_{el}^* = \mu_{el}/(k_B T)$, where l_0 is the grid spacing.

Considering a model system, the chemical free energy density, f , is described by a double-well potential with minima at equilibrium compositions of ± 1.0 :

$$f^*(X) = -\frac{1}{2}X^2 + \frac{1}{4}X^4 \quad (5)$$

2.2. Elastic energy in constrained films

If we assume that the variation of the stress-free lattice parameter, a , with composition is linear, i.e. it obeys the Vegard's law, the local stress-free strain caused by compositional inhomogeneity is given by [39]

$$\varepsilon_{ij}^0(\bar{r}) = \varepsilon_0 \delta X(\bar{r}) \delta_{ij} \quad (6)$$

where $\varepsilon_0 = (1/a)(da/dX)$ is the compositional expansion coefficient of the lattice parameter and δ_{ij} is the Kronecker–Delta function.

In the linear elasticity, the stress σ_{ij} is related to the elastic strain by the Hooke's law:

$$\sigma_{ij} = c_{ijkl}(\varepsilon_{kl}(\bar{r}) - \varepsilon_{kl}^0(\bar{r})) \quad (7)$$

where c_{ijkl} is the elastic stiffness which gives the crystal elastic constants and $\varepsilon_{kl}(\vec{r})$ is the total strain measured with respect to a reference lattice. The effect of composition on the elastic constants is neglected. The total strain can be separated into homogeneous and heterogeneous strains [2]:

$$\varepsilon_{ij}(\vec{r}) = \bar{\varepsilon}_{ij} + \delta\varepsilon_{ij}(\vec{r}) \quad (8)$$

where the heterogeneous strain, $\delta\varepsilon_{ij}(\vec{r})$, is defined so that

$$\int_V \delta\varepsilon_{ij}(\vec{r}) d^3r = 0 \quad (9)$$

The homogeneous strain is the uniform macroscopic strain characterizing the macroscopic shape and volume change associated with the total strain. The strain and displacement relationship gives the following equation:

$$\delta\varepsilon_{ij}(\vec{r}) = \frac{1}{2} \left[\frac{\partial u_i(\vec{r})}{\partial r_j} + \frac{\partial u_j(\vec{r})}{\partial r_i} \right] \quad (10)$$

where $u_i(\vec{r})$ denotes the i th component of displacement.

The mechanical equilibrium equations with respect to elastic displacements are expressed as

$$\frac{\partial \sigma_{ij}}{\partial r_j} = 0 \quad (11)$$

where r_j is the j th component of \vec{r} . The stress-free boundary condition at the top surface of a film is given by

$$\sigma_{i3}|_{x_3=h_f} = 0 \quad (12)$$

where h_f is the film thickness along x_3 direction as shown in Fig. 1. Since the elastic perturbation resulted from the heterogeneous strain disappears in the substrate far from the film–substrate interface, the following condition is used to describe the constraint of the substrate

$$u_i|_{x_3=-h_s} = 0 \quad (13)$$

where h_s is the distance from the film–substrate interface into the sufficiently thick substrate, beyond which the elastic deformation is ignored (see Fig. 1).

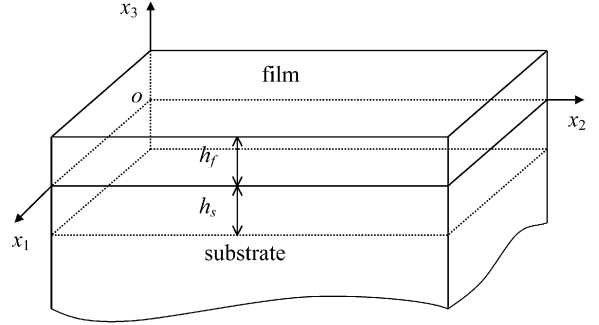


Fig. 1. Schematic illustration of a thin film coherently constrained by a substrate.

To solve Eqs. (11)–(13), two elastic solutions are superposed [37]. First solution is from Khachaturyan’s microelasticity theory [2] within $0 < x_3 < h_f$ and second one is from the elastic solution in an infinite plate of thickness $h_f + h_s$, satisfying the two boundary conditions. Consequently, the elastic energy in the constrained thin film can be calculated from Eqs. (7), (8) and (10).

2.3. Three-dimensional simulation of spinodal decomposition

Taking Fourier-transform of Eq. (4), we have the temporal evolution of the composition wave amplitude, $X(\vec{g}^*, t^*)$,

$$\frac{\partial X(\vec{g}^*, t^*)}{\partial t^*} = -(g^*)^2 \left[\left(\frac{df^*(X)}{dX} \right)_{\vec{g}^*} + \alpha^*(g^*)^2 X(\vec{g}^*, t^*) + \mu_{ei}^*(\vec{g}^*) \right] \quad (14)$$

where g^* is the magnitude of \vec{g}^* , a vector in the Fourier space, $X(\vec{g}^*, t^*)$, $(df^*(X)/dX)_{\vec{g}^*}$ and $\mu_{ei}^*(\vec{g}^*)$ are the Fourier transforms of $X(\vec{r}^*, t^*)$, $(df^*(X)/dX)_{\vec{r}^*}$, and $\mu_{ei}^*(\vec{r}^*)$, respectively. The above equation can be efficiently solved using a semi-implicit method [39,40]. More precisely,

$$X^{n+1}(\vec{g}^*) = \quad (15)$$

$$\frac{(4X^n(\vec{g}^*) - X^{n-1}(\vec{g}^*)) / 3 - (2/3)\Delta t^* (g^*)^2 [2(\mu^*(\vec{g}^*))^n - (\mu^*(\vec{g}^*))^{n-1}]}{1 + (2/3)\Delta t^* \alpha^*(g^*)^4}$$

where $\mu^* = df^*(X)/dX + \mu_{el}^*$ and Δt^* is the time step for integration.

For time discretization, a second-order backward difference scheme is applied. For spatial discretization, a Fourier-spectral method is used in x_1 and x_2 direction, and since the zero-flux boundary conditions at film surface and film/substrate interface cannot be satisfied by a Fourier expansion, a second-order finite difference method with Fast Fourier Transform (FFT) is used in the x_3 direction.

In the computer simulation, $128 \times 128 \times 48$ discrete grid points are used where $h_t = 32l_0$, and periodic boundary conditions are applied along x_1 and x_2 axes. The dimensionless grid spacing in real space is chosen to be $\Delta x_1/l_0 = \Delta x_2/l_0 = \Delta x_3/l_0 = 1.0$ and Δt^* is chosen to be 0.05. The dimensionless gradient energy coefficient, α^* , is chosen to be 0.6. The interface energy between decomposed phases is assumed to be isotropic. The overall reduced composition used in this study is an off-critical composition of -0.3 . A small compositional fluctuation is applied to initiate the decomposition process by the random number generation at the initial stage. The elastic constants used for the film are $C_{11} = 375$, $C_{12} = 125$, $C_{44} = 125$ for an isotropic cubic material, and $C_{11} = 375$, $C_{12} = 250$, $C_{44} = 125$ for an anisotropic cubic material, all in units of $N_V k_B T$ where N_V is the number of atoms per unit volume. Same elastic constants are used for the substrate. Note that the anisotropy given by $(C_{11} - C_{12} - 2C_{44})/C_{44}$ is negative. The film is assumed to be coherent with the substrate and has the same elastic constants as the substrate.

3. Results and discussion

A typical temporal evolution of the phases during the spinodal decomposition in bulk AB binary alloy system is shown in Fig. 2. In this case $64 \times 64 \times 64$ grid points are used. The solid region corresponds to the higher concentration (B-rich) and transparent region corresponds to the lower concentration (A-rich). A small compositional fluctuation leads to a spontaneous phase separation, producing a three-dimensionally interconnected microstructure as shown in the figure.

The local stress field in the thin film is caused by the local compositional inhomogeneity with

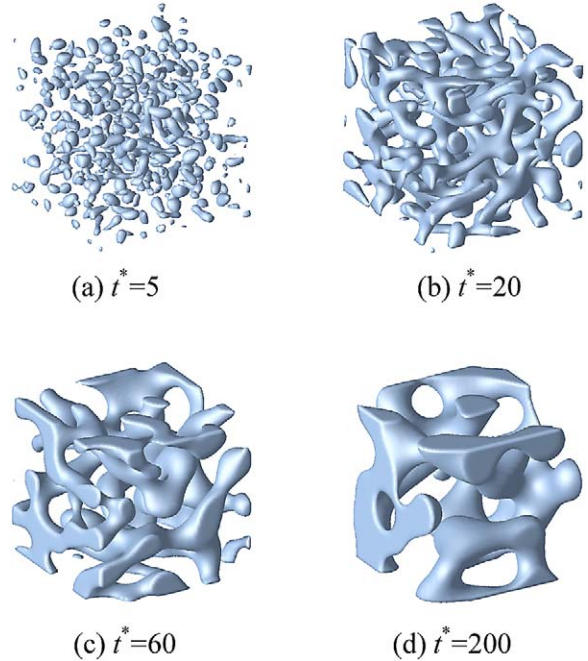


Fig. 2. Temporal evolution of the phases during the spinodal decomposition in bulk AB binary alloy system.

coherent interfaces between decomposed phases. If we assume the atomic sizes of A and B atoms in the film are same and there is no elastic constraint of the film by the substrate, the spinodal decomposition is driven by the bulk chemical free energy and the interface energy without the elastic energy. Fig. 3 shows the temporal evolution of the phases during the spinodal decomposition in the thin film without the elastic energy. The solid region corresponds to the higher concentration (B-rich) and the bottom plate is the substrate. The decomposition occurs homogeneously throughout the film from the initial stage. From the three-dimensional observation, B-rich phases are interconnected randomly, i.e. without any preferred direction of interconnection or layer formation. Columnar shape is observed near the film/substrate interface and film surface.

Columnar morphology results from the finite film thickness and the zero-flux boundary condition at the film/substrate interface and film surface. As the film thickness become thinner (see Fig. 4), the three-dimensional diffusional process

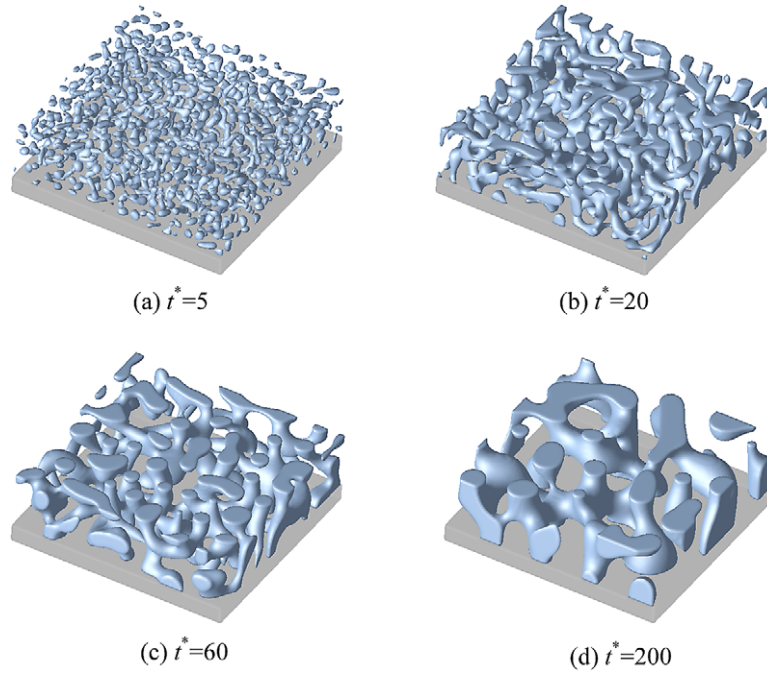


Fig. 3. Temporal evolution of the phases during the spinodal decomposition in thin film without the elastic energy.

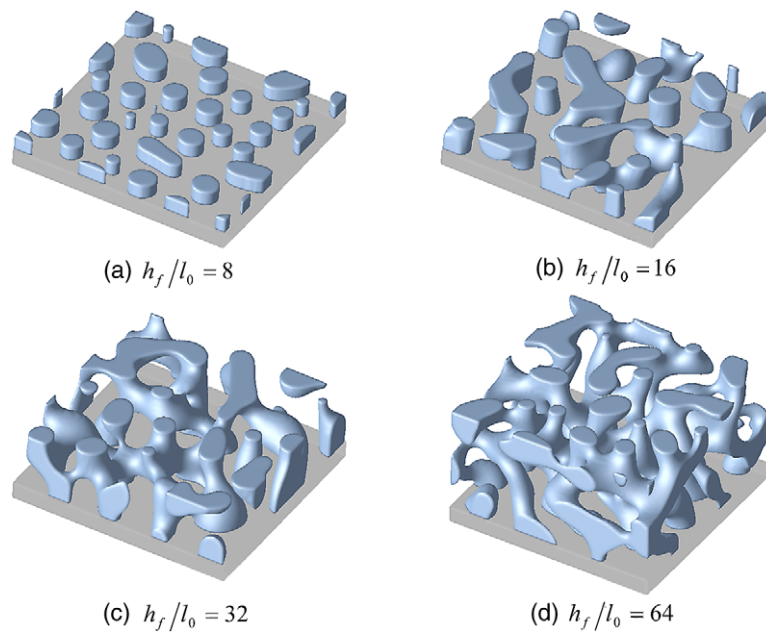


Fig. 4. The phase morphology in thin films without the elastic energy at various film thickness of (a) $h_f/l_0 = 8$, (b) $h_f/l_0 = 16$, (c) $h_f/l_0 = 32$ and (d) $h_f/l_0 = 64$.

becomes approximately two-dimensional along x_1 and x_2 directions. Fig. 4(a) shows a fully columnar morphology in a very thin film with $h_f/l_0 = 8$. It has little morphological change along x_3 direction. As the film thickness increases, the morphology becomes more three-dimensional and interconnected. In a thicker film with $h_f/l_0 = 64$, Fig. 4(d) shows a microstructure similar to that of bulk material shown in Fig. 2.

When the film thickness is given as $h_f/l_0 = 8$, the composition determines whether the microstructure becomes isolated columnar or interconnected. The overall reduced composition was decreased to -0.5 and increased to 0.0 from the original composition of -0.3 in order to show the effect of composition on the decomposed morphology. The overall composition determines the equilibrium volume fraction. Fig. 5(a) and (b) show the microstructure evolution with the overall composition of -0.5 . Throughout the decomposition process, B-rich phase regions are isolated because of a low volume fraction. The volume fraction of the B-rich phase in Fig. 5(b) is 0.20 and the shape is cylindrical to reduce interface energy. When the overall composition was increased to 0.0 , as shown in Fig. 6(a) and (b), the decomposition proceeds with the finely interconnected three-dimensional structure first and then leads to the interconnected columnar structure during coarsening. Volume fractions of both B-rich and A-rich phases are 0.45 and the fraction of the interface region amounts to 0.10 due to the assumption of diffuse interface in this model.

Fig. 7 shows the temporal evolution of the phases during the spinodal decomposition of an

elastically isotropic material of which the compositional expansion coefficient of the lattice parameter is 0.02 . The positive compositional expansion coefficient means the size of B atom is larger than that of A atom. The initial decomposition starts at the film surface where it is easier to relieve the local stress field accompanied by the decomposition. Compared to Fig. 3, decomposed phases have a slight tendency to align parallel to the x_1x_2 plane due to the initial layer formation at the film surface.

Fig. 8 shows the temporal evolution of the phases during the spinodal decomposition of an elastically anisotropic material of which the compositional expansion coefficient of the lattice parameter is 0.02 . From the early stage decomposition at the film surface, decomposed phases have a tendency to align along $\langle 100 \rangle$ directions. For a cubic alloy with negative elastic anisotropy, $\langle 100 \rangle$ directions are elastically soft directions, and morphological alignment along those directions results in a decrease in the elastic energy [40]. As the B-rich domain coarsens, the morphology not only shows a strong $\langle 100 \rangle$ alignment in the x_1x_2 plane, but also shows a layered structure along x_3 direction. The B-rich phase seldom interconnects each other along x_3 direction at the composition of -0.3 and the film thickness of $h_f/l_0 = 32$. The increase in the composition provides morphological alignment along all three directions. Layered structure along x_3 direction cannot be observed at the composition of 0.0 . If the composition decreases below -0.3 , the number of B-rich layers in the layered structure reduces due to the decrease in the volume fraction of B-rich phase.

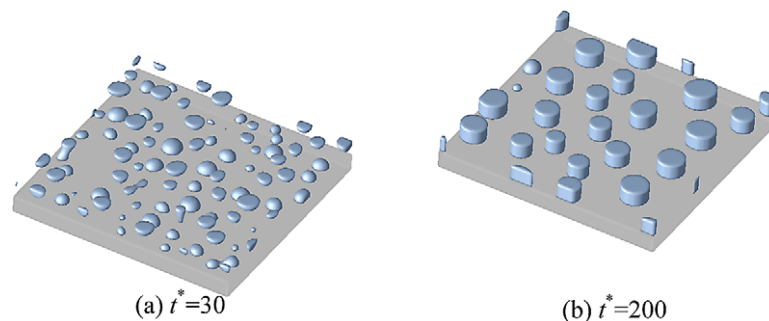


Fig. 5. Microstructure evolution with the overall reduced composition of -0.5 at (a) $t^* = 30$ and (b) $t^* = 200$.

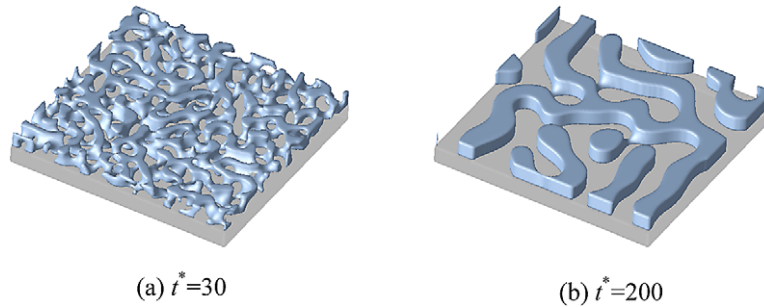


Fig. 6. Microstructure evolution with the overall reduced composition of 0.0 at (a) $t^* = 30$ and (b) $t^* = 200$.

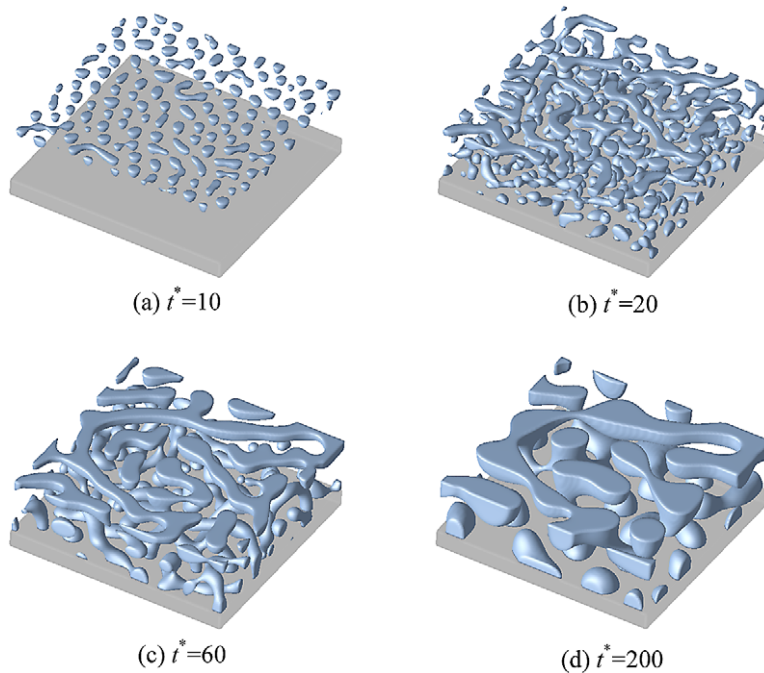


Fig. 7. Temporal evolution of the phases during the spinodal decomposition in an elastically isotropic film.

The pictures of spinodally phase-separated microstructures presented in Figs. 7 and 8 do not take into account the local displacements. As a result of compositional fluctuation with different atomic sizes, an initially atomically flat surface is expected to become rough. The surface topology change due to the phase separation can be determined from the elastic solutions for a given phase-separated microstructure. Fig. 9 shows an example of the displacements along the x_3 direction on the surface for the two-phase structure shown in Fig.

8(d). As expected from the larger size of B atom, the displacements within B-rich phase regions are positive whereas those within A-rich regions are negative, ranging from maximum 0.8349 to minimum -0.7625 .

The formation of layered structure in Fig. 8 can be effectively observed in a two-dimensional x_1x_3 section with increasing the time as shown in Fig. 10. The bright and dark regions correspond to the B-rich and A-rich regions, respectively. The B-rich region forms at the film surface first and the A-

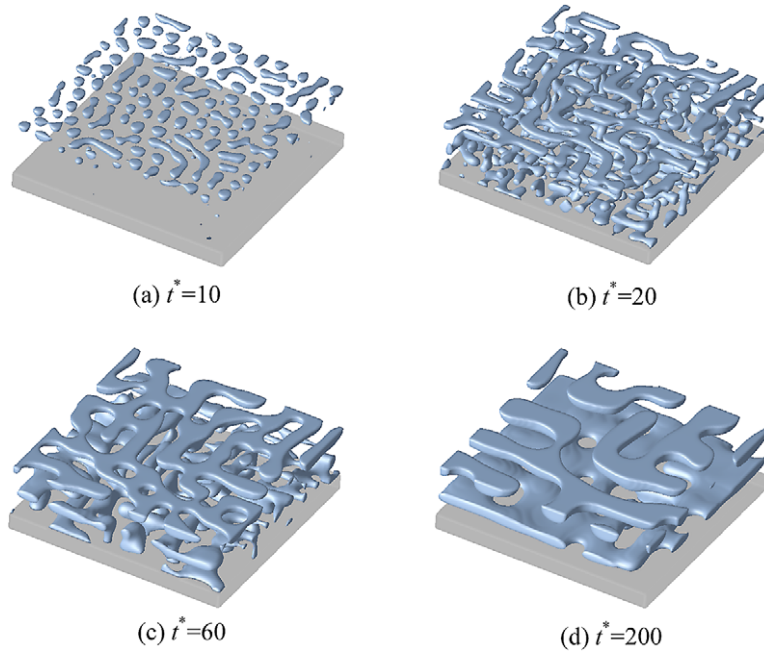


Fig. 8. Temporal evolution of the phases during the spinodal decomposition in an elastically anisotropic film.

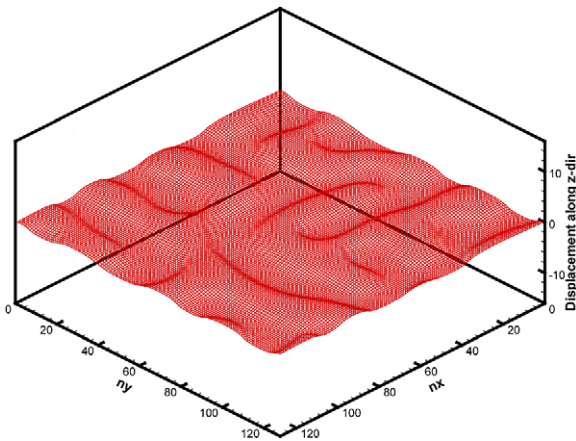


Fig. 9. Displacement pattern of the x_3 component on the surface.

rich region forms next to the surface layer where B component is depleted. The B-rich region cannot form right beneath the surface layer because the compressive stress field overlaps. The layer forming process propagates gradually with time from the film surface to the film/substrate interface. With forming the layered structure, the alternating

compressive and tensile stress fields develop without causing a macroscopic displacement in the x_1 or x_2 direction. The phase separation procedure observed in Fig. 10 can be thought as a kind of surface-directed spinodal decomposition, driven by the elastic effect. Instead of an initial surface layer formed by a preferred component to reduce the surface energy in usual surface-directed spinodal decomposition [31], the surface, where the strain energy barrier is lowest, is favored for the initial phase separation. The difference between two different mechanisms lies in their morphology of surface layer. The surface-directed spinodal decomposition driven by the surface energy effect will produce a wholly planar layer of one phase that is favorable in terms of surface energy reduction at the film surface, in the early stage of phase separation [32,34]. The spinodal wave vector is more one-dimensional compared to that in the surface-directed spinodal decomposition driven by the elastic effect.

Fig. 11(a) and (b) show profiles of averaged compositions over x_1x_2 plane with respect to the position along x_3 direction from the film/substrate

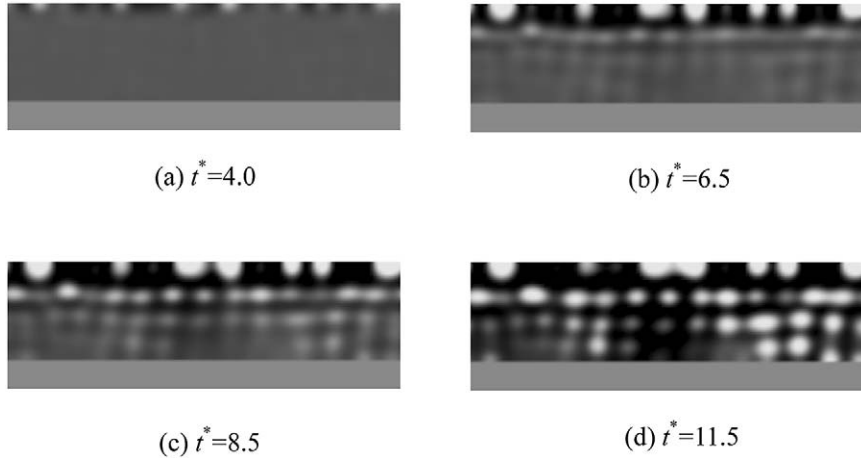


Fig. 10. Sequential formation of the layered structure observed in the x_1x_3 section at (a) $t^* = 4.0$, (b) $t^* = 6.5$, (c) $t^* = 8.5$ and (d) $t^* = 11.5$.

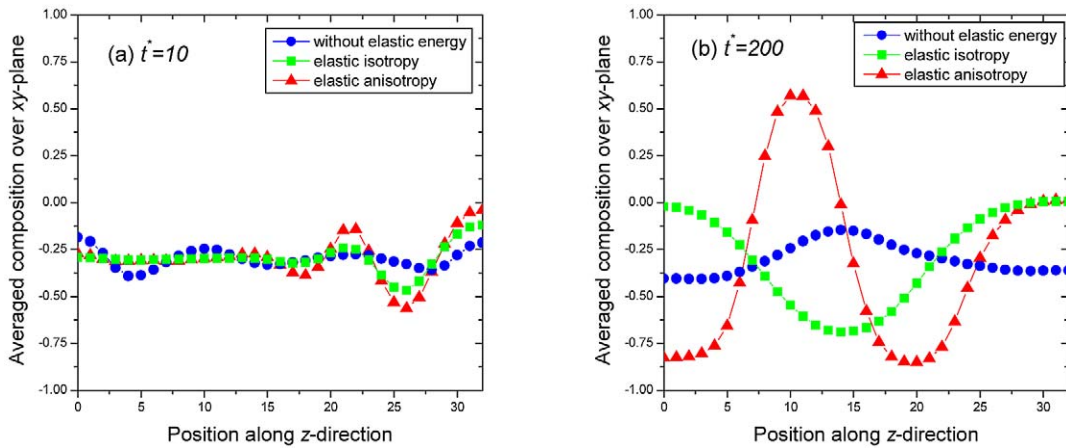


Fig. 11. Profiles of averaged compositions over x_1x_2 plane with respect to the position along x_3 direction from the film/substrate interface to the film surface at (a) $t^* = 10$ and (b) $t^* = 200$.

interface to the film surface. When $t^* = 10$ in Fig. 11(a), the coherency strain energy causes compositional fluctuations at the film surface first and the compositions near the film/substrate interface are still homogeneous in the elastically isotropic and anisotropic materials. As to the film without elastic energy, the compositional fluctuation exists throughout the film thickness. When $t^* = 200$ in Fig. 11(b), all composition profiles fluctuate. Especially the elastically anisotropic material shows largest fluctuation along x_3 direction forming layered structure. The coherency strain

energy and elastic anisotropy increase the tendency of the layer formation.

The volume fraction change of the B-rich phase is drawn in Fig. 12 as a function of time in order to show the effect of coherency strain energy on the decomposition kinetics and decomposed volume fractions. Without elastic energy, the film decomposes abruptly at the initial stage right after the initial compositional fluctuation. The strain energy in elastically isotropic and anisotropic materials obviously retards the decomposition process. The elastically anisotropic material decom-

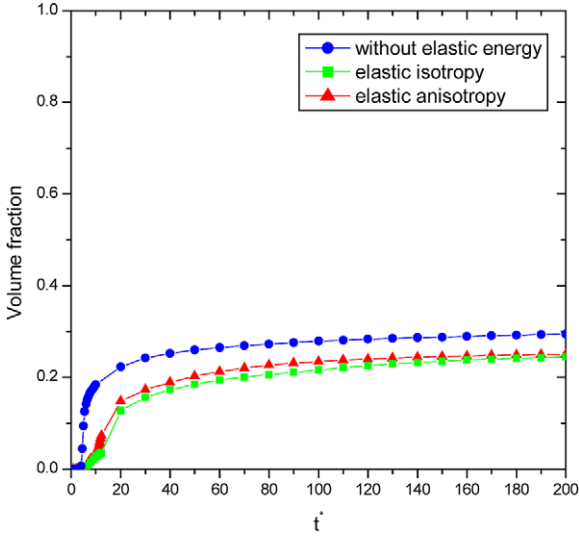


Fig. 12. Volume fraction change of the B-rich phase with respect to the time.

poses slightly faster than the isotropic material because the elastic anisotropy provides $\langle 100 \rangle$ directions that have low strain energy. The slow decomposition kinetics in the film with the coherency strain energy is due to the decrease in the driving force of spinodal decomposition as it was pointed out long time ago by Cahn [41]. We consider a one-dimensional elastic deformation of a film constrained by a rigid substrate. The free energy increase due to coherency strain energy is given by

$$\Delta f^* = \frac{1}{2} E^* [\varepsilon_0 (X - X_0)]^2 \quad (16)$$

where E^* is a dimensionless Young's modulus of the film, and ε_0 is the compositional expansion coefficient of the lattice parameter. Adding Eq. (16) to the chemical free energy density gives

$$f^*(X) = -\frac{1}{2} X^2 + \frac{1}{4} X^4 + \frac{1}{2} E^* \varepsilon_0^2 (X - X_0)^2 \quad (17)$$

Eq. (17) is plotted in Fig. 13 with various amounts of compositional mismatch, ε_0 . The overall composition X_0 is the critical composition, i.e. $X_0 = 0$. A typical value of E^* is taken as 250. As the ε_0 increases, the driving force for the spinodal decomposition decreases due to the increased

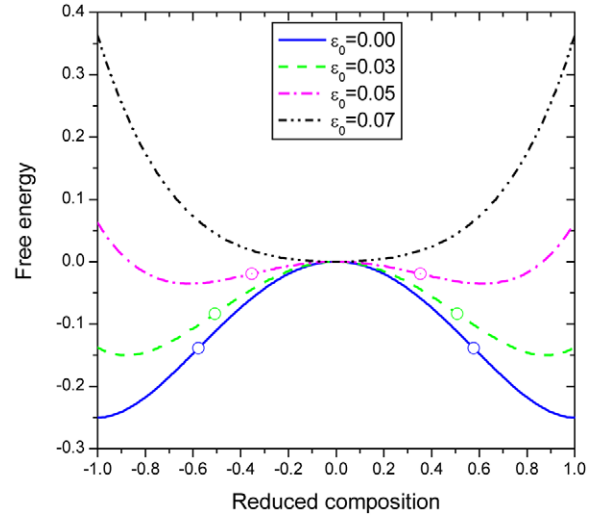


Fig. 13. Change of the free energy function with respect to the amount of compositional mismatch, ε_0 .

coherency strain energy and the spinodal region between the circles in each curve reduces. The second derivative of the free energy density becomes zero at the circles where $X = \pm\sqrt{(1 - E^* \varepsilon_0^2)/3}$. If the ε_0 is larger than $1/\sqrt{E^*}$, the system is outside of the miscibility gap ($\varepsilon_0 = 0.07$ in the figure). The decrease in the driving force of the spinodal decomposition with coherency strain energy makes the decomposition kinetics slower than that without strain energy.

Fig. 14 shows the morphology change caused by reducing h_s for an elastically anisotropic material. The reduction of h_s indicates an increased hardness of the substrate material. Note that $h_s/l_0 = 10$ in Fig. 8. The h_s is decreased as $h_s/l_0 = 5$ in Fig. 14(a) and $h_s/l_0 = 1$ in Fig. 14(b). As the h_s decreases, one B-rich layer close to the film/substrate interface becomes entirely a B-rich plane, while the B-rich phase region in the other layer shrinks at the film surface. A strong constraint by the hard substrate in Fig. 14(b) makes the concentration distribution uniform near the film/substrate interface.

4. Conclusions

A three-dimensional phase-field model is employed to study the morphological evolution

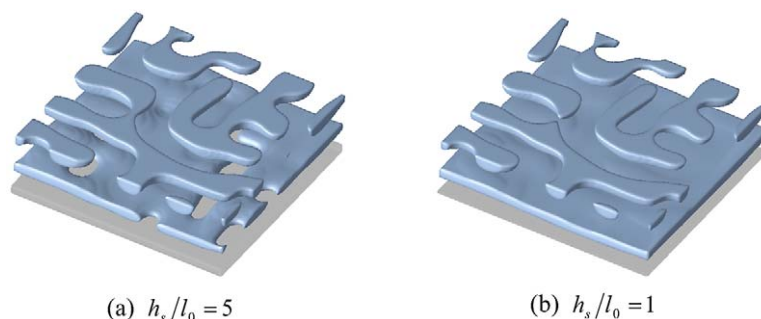


Fig. 14. Morphology change in the elastically anisotropic film caused by the h_s decrease: (a) $h_s/l_0 = 5$ and (b) $h_s/l_0 = 1$.

during spinodal decomposition in a binary alloy thin film elastically constrained by a substrate. Without coherency strain, the compositional fluctuation simultaneously occurs in the whole film from the initial stage of the spinodal decomposition. The morphology of decomposed phases depends on the film thickness and the composition. The tendency of forming isolated columnar structure is enhanced as the film thickness decreases and the composition becomes more off-critical within the unstable part of the miscibility gap. When the coherency strain is introduced, the phase separation follows the mechanism of surface-directed spinodal decomposition, driven by the elastic energy effect, within a certain range of the composition. The resultant microstructure in an elastically anisotropic film is alternately aligned layer structure parallel to the film surface along the x_3 direction. Due to the negative elastic anisotropy in the cubic alloy, decomposed phases align along elastically soft $\langle 100 \rangle$ directions to reduce the elastic energy. The increased substrate hardness affects the morphology. The coherency strain energy in elastically isotropic and anisotropic materials delays the kinetic process of the spinodal decomposition due to reduced driving force for the decomposition.

Acknowledgements

Authors are grateful for the financial support for this research by the National Research Laboratory Project through the Ministry of Science and Technology, and by the US National Science Foun-

dation under grant numbers DMR-01-22638 and DMS-0074283.

References

- [1] Cahn JW. *Trans AIME* 1968;242:166.
- [2] Khachaturyan AG. *Theory of structural transformations in solids*. New York: Wiley, 1983.
- [3] Cahn JW. *Acta Metall* 1962;10:907.
- [4] Cahn JW, Larché F. *Acta Metall* 1984;32:1915.
- [5] Larché FC, Cahn JW. *Acta Metall* 1985;33:331.
- [6] Johnson WC, Voorhees PW. *Met Trans A* 1987;18:1213.
- [7] Johnson WC. *Met Trans A* 1987;18:1093.
- [8] Rogers TM, Elder KR, Desai RC. *Phys Rev B* 1988;37:9638.
- [9] Onuki A. *J Phys Soc Jpn* 1989;58:3065.
- [10] Nishimori H, Onuki A. *Phys Rev B* 1990;42:980.
- [11] Chen LQ, Wang YZ, Khachaturyan AG. *Phil Mag Lett* 1991;64:241.
- [12] Wang YZ, Chen LQ, Khachaturyan AG. *Acta Metall Mater* 1993;41:279.
- [13] Abinandanan TA, Johnson WC. *Acta Metall Mater* 1993;41:17.
- [14] Thompson ME, Su CS, Voorhees PW. *Acta Metall Mater* 1994;42:2107.
- [15] Sagui C, Somoza AM, Desai R. *Phys Rev E* 1994;50:4865.
- [16] Fratzl P, Penrose O. *Acta Metall Mater* 1995;43:2921.
- [17] Koyama T, Miyazaki T, Mebed AE. *Metal Mater Trans A* 1995;26:2617.
- [18] Lee JK. *Metal Mater Trans A* 1995;27:1449.
- [19] Jou HJ, Leo PH, Lowengrub JS. *J Comput Phys* 1997;131:109.
- [20] Sagui C, Orlikowski D, Somoza A, Roland C. *Phys Rev E* 1998;58:569.
- [21] Orlikowski D, Sagui C, Somoza A, Roland C. *Phys Rev B* 1999;59:8646.
- [22] Chen LQ. In: Turchi PEA, Gonis A, editors. *Phase trans-*

- formations and evolution in materials. Warrendale, PA: The Minerals, Metals & Materials Society; 2000. p. 209.
- [23] Larché FC, Cahn JW. *Acta Metall Mater* 1992;40:947.
- [24] Cahn JW, Kobayashi R. *Acta Metall Mater* 1995;43:931.
- [25] Abadias G, Marty A, Gilles B. *Acta Mater* 1998;46:6403.
- [26] Binder K. *J Non-Equilib Thermodyn* 1998;23:1.
- [27] Greaney PA, Clemens BM, Nix WD, Chrzan, DC. Private communication, 2003.
- [28] Johnson WC, Wise SM. *Appl Phys Lett* 2002;81:919.
- [29] Léonard F, Desai R. *Phys Rev B* 1998;58:8277.
- [30] Leo PH, Johnson WC. *Acta Mater* 2001;49:1771.
- [31] Puri S, Frisch HL. *J Phys: Condens Matter* 1997;9:2109.
- [32] Brown G, Chakrabarti A. *Phys Rev A* 1992;46:4829.
- [33] Geng C, Chen LQ. *Surf Sci* 1996;355:229.
- [34] Puri S, Binder KJ. *Stat Phys* 1994;77:145.
- [35] Ball RC, Essery RLH. *J Phys: Condens Matter* 1990;2:10303.
- [36] Li YL, Hu SY, Liu ZK, Chen LQ. *Appl Phys Lett* 2001;78:3878.
- [37] Li YL, Hu SY, Liu ZK, Chen LQ. *Acta Mater* 2002;50:395.
- [38] Seol DJ, Hu SY, Li YL, Chen LQ, Oh KH. *Mater Sci Forum* 2002;1645:408–12.
- [39] Hu SY, Chen LQ. *Acta Mater* 2001;49:1879.
- [40] Chen LQ, Shen J. *Comput Phys Commun* 1998;108:147.
- [41] Cahn JW. *Acta Metall* 1962;10:907.